

Article

Fracture Propagation Laws and Influencing Factors in Coal Reservoirs of the Baode Block, Ordos Basin

Qingfeng Zhang¹, Yongchen Li¹, Ziling Li¹, Yanbin Yao^{2,3} , Fengfeng Du^{2,3}, Zebin Wang¹, Zhihao Tang¹, Wen Zhang¹ and Shutong Wang^{2,3,*}

¹ PetroChina Coalbed Methane Company Limited, Beijing 100028, China; zqf2012@petrochina.com.cn (Q.Z.); lyc1987@petrochina.com.cn (Y.L.); lzl_cbm@petrochina.com.cn (Z.L.); wzb0715@petrochina.com.cn (Z.W.); tzh_cbm@petrochina.com.cn (Z.T.); zw1229@petrochina.com.cn (W.Z.)

² School of Energy Resource, China University of Geosciences, Beijing 100083, China; yyb@cugb.edu.cn (Y.Y.); dff9803@163.com (F.D.)

³ Beijing Key Laboratory of Unconventional Natural Gas Geological Evaluation and Development Engineering, China University of Geosciences, Beijing 100083, China

* Correspondence: wstylyh@163.com

Abstract: The expansion of hydraulic fractures in coalbed methane (CBM) reservoirs is key to effective stimulation, making it essential to understand fracture propagation and its influencing factors for efficient resource development. Using petrological characteristics, logging data, microseismic monitoring, and fracturing reports from the Baode Block on the eastern Ordos Basin, this study systematically investigates the geological and engineering factors influencing hydraulic fracture propagation. The real-time monitoring of fracture propagation in 12 fractured wells was conducted using microseismic monitoring techniques. The results indicated that the fracture orientations in the study area ranged from NE30° to NE60°, with fracture lengths varying between 136 and 226 m and fracture heights ranging from 8.5 to 25.3 m. Additionally, the fracturing curves in the study area can be classified into four types: stable, descending, fluctuating, and falling. Among these, the stable and descending types exhibit the most effective fracture propagation and are more likely to generate longer fractures. In undeformed–cataclastic coals and bright and semi-bright coals, long fractures are likely to form. When the Geological Strength Index (GSI) of the coal rock ranges between 60 and 70, fracture lengths generally exceed 200 m. When the coal macrolithotype index (S_m) is below 2, fracture lengths typically exceed 200 m. When the difference between the maximum and minimum horizontal principal stresses exceeds 5 MPa, fractures with length >180 m are formed, while fracture heights generally remain below 15 m. From an engineering perspective, for the study area, hydraulic fracturing measures with a preflush ratio of 20–30%, an average sand ratio of 13–15%, and a construction pressure between 15 MPa and 25 MPa are most favorable for coalbed methane production.

Keywords: coalbed methane; hydraulic fracturing; fracture propagation; coal structure; coal macrolithotype; in situ stress



Citation: Zhang, Q.; Li, Y.; Li, Z.; Yao, Y.; Du, F.; Wang, Z.; Tang, Z.; Zhang, W.; Wang, S. Fracture Propagation Laws and Influencing Factors in Coal Reservoirs of the Baode Block, Ordos Basin. *Energies* **2024**, *17*, 6183. <https://doi.org/10.3390/en17236183>

Academic Editor: Nikolaos

Koukouzas

Received: 10 November 2024

Revised: 2 December 2024

Accepted: 5 December 2024

Published: 8 December 2024



Copyright: © 2024 by the authors. Licensee MDPI, Basel, Switzerland. This article is an open access article distributed under the terms and conditions of the Creative Commons Attribution (CC BY) license (<https://creativecommons.org/licenses/by/4.0/>).

1. Introduction

In the latest round of oil and gas resource evaluation in China conducted in 2016, the total reserves of coalbed methane (CBM) resources located at depths shallower than 2000 m were approximately 29.8 trillion cubic meters, with technically recoverable resources estimated at around 12.5 trillion cubic meters [1]. However, China's CBM production rates from individual wells are quite low, primarily because large-scale development has focused on areas rich in mid- to high-rank coals, which typically exhibit lower permeability compared to low-rank coals [2,3]. Therefore, the targeted hydraulic fracturing of CBM reservoirs is essential for achieving cost-effective development and maximizing energy utilization [4,5].

Hydraulic fracturing is a mature technology that has been commercially utilized since the late 1940s. In recent years, researchers have achieved significant advancements in understanding the effects of fracture extension through the lenses of solid mechanics [6–8], fluid mechanics [9–11], and construction parameter optimization [12,13]. Compared to shale and sandstone, coal rock possesses a lower modulus of elasticity, a higher Poisson's ratio, and greater non-homogeneity, resulting in the more complex formation and extension of hydraulic fractures [14–16]. Through extensive on-site monitoring and simulation analysis, previous researchers have identified a range of factors and principles that influence the expansion of fractures in coal reservoirs. For instance, Zhong et al. [17] found that the magnitude of the horizontal principal in situ stress difference affects the directional extension of hydraulic fractures. Additionally, natural fractures play a crucial role in hydraulic fracture propagation, as they can either facilitate communication, allow penetration, or lead to capture by hydraulic fractures [18,19]. Zhao et al. [20] found that the coal macrolithotype influences both the fracture morphology and proppant distribution. Yushi et al. [21] demonstrated that elasticity, strength, and stress anisotropy affect fracture extension in simulations. However, previous studies have primarily focused on the theoretical examination of individual factors, lacking comparative analyses that align with actual production scenarios. As a result, their findings often fail to effectively guide yield enhancement measures. Furthermore, the fracturing process must be tailored to the specific characteristics of different coalbeds [22–24].

Using the Baode Block as a case study, this research analyzes the impact of geological and engineering factors on hydraulic fracture expansion behavior through microseismic monitoring technology, well logging data, and fracturing operation reports. The aim is to enhance fracturing effectiveness and economic benefits, while also providing a reference for CBM development.

2. Geological Settings

The Baode Block is located in the northern part of the eastern margin of the Ordos Basin in China (Figure 1a). This block is directly influenced by the uplift of the Lvliang Mountains, with the dominant structural line trending approximately north–south, resulting in a monocline structure that dips westward. The formation's dip angle is generally gentle, ranging from 1° to 2° , with local areas exhibiting dips of 5° to 10° . Overall, the region displays a transitional basin margin structural type, characterized by folds and faults primarily in the central and southern parts, mostly oriented in the NNE or NE directions. The regional tectonic stress field is mainly influenced by the Yanshan and Himalayan movements, with the maximum principal stress during the Yanshan period oriented at $NW324^\circ$ and at $NE57^\circ$ during the Himalayan period [25]. The Upper Paleozoic coal-bearing sequences include the Carboniferous Benxi Formation and the Permian Shanxi and Taiyuan Formations [26]. The main coal seams of 4 + 5# and 8 + 9# are mainly developed in the study area, of which the 4 + 5# coal seam of the Shanxi Formation is the primary focus of this study, with burial depths ranging from 445.6 m to 1116.8 m and seam thicknesses between 3.5 m and 15 m, averaging 7.2 m. The maximum vitrinite reflectance (R_o, \max) of the samples ranges from 0.7% to 0.9%, indicating that the coal type is gas coal. Additionally, 2#, 3#, 6#, and 7# non-dominant coal seams are developed above and below the 4 + 5# seams (Figure 1b), with an average spacing of 5 to 25 m. According to the experience from coalbed methane well development, these coal seams can be combined for extraction [27].

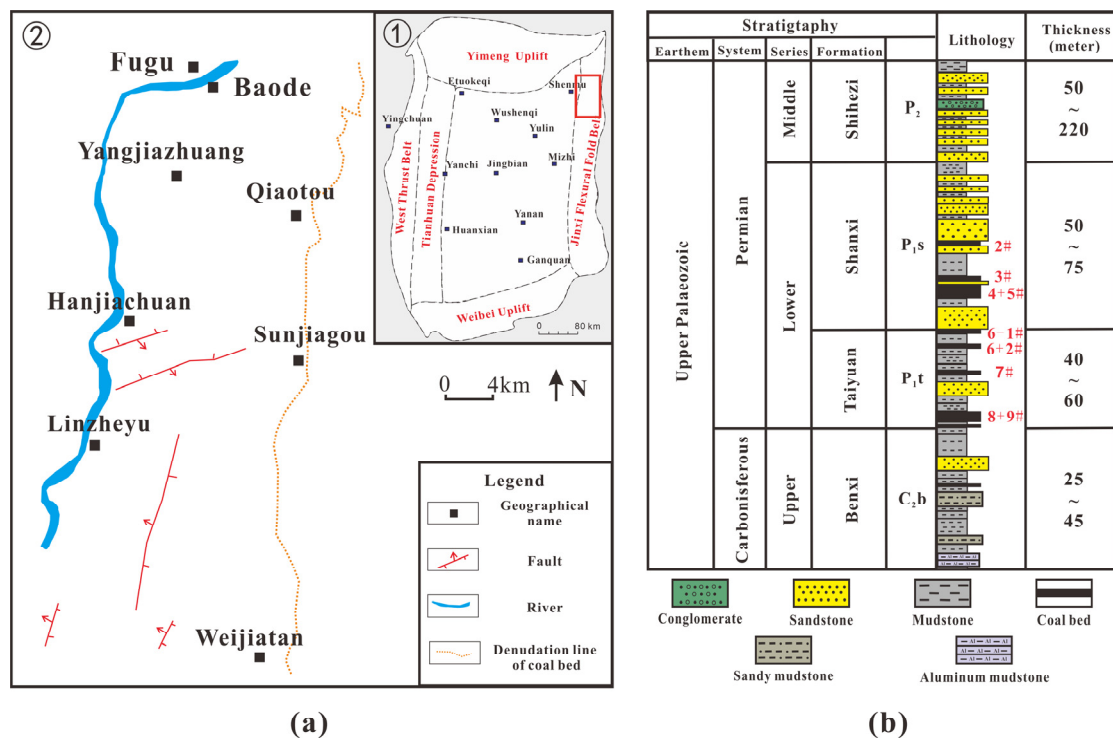


Figure 1. (a) Outline map of Baode Block (the red rectangle show the study area) (from Xu et al. [28]); (b) stratigraphic column of the Paleozoic strata in the Baode Block area (modified from Liu et al. [26]).

3. Hydraulic Fracturing and Monitoring Methods

The basic data involved in this work were provided by the Xinzhou Gas Mining Management Area of PetroChina Coalbed Methane Company Limited, including hydraulic fracturing reports and production data from 589 CBM wells and 12 microseismic monitoring reports.

3.1. Hydraulic Fracturing

The fracturing process in the study area primarily utilizes simulated formation water combined with drag-reducing additives, with very few wells employing slickwater fracturing fluids. Consequently, this paper focuses on analyzing the fracture extension laws and influencing factors associated with the use of simulated formation water as the fracturing fluid. The proppants selected for the study area were all quartz sand, with particle sizes of 30/50 mesh (0.3–0.6 mm), 40/70 mesh (0.3–0.4 mm), and 70/140 mesh (0.1–0.2 mm). The total fracturing fluid volume of the 12 fractured wells in the study area ranged from 917 to 3061 m³, the total sand addition volume ranged from 57.5 to 396 m³, the preflush fluid volume ranged from 235.5 to 339 m³, the average sand ratio ranged from 9% to 17.94%, and the range of variation in the construction pressure ranged from 8.6 to 38.6 MPa. During hydraulic fracturing operations, key parameters such as sand volume, liquid volume, and displacement were obtained through real-time monitoring of surface equipment [29]. Wellhead pressure is measured using pressure sensors, liquid volume is tracked with flow meters, and sand volume is determined by monitoring the proppant flow rate in the slurry. These data are critical for evaluating the fracturing process and ensuring its smooth execution.

3.2. Microseismic Monitoring

Microseismic monitoring is commonly used to invert the characteristics of fracture extension, enabling the determination of the propagation direction and influence the range of hydraulic fractures by observing and analyzing the microseismic events generated during production activities [30]. During the fracturing process, microseismic monitoring can track

the length, height, direction, and extension of fractures in the formation, providing insights into the spatial propagation characteristics of the fractures [31,32]. Typically, microseismic data are collected through a combined ground and in-well monitoring approach. On the ground, geophones are deployed radially, while in neighboring wells, three-component geophones are placed downhole to capture microseismic signals around the target layer of the fracturing well. The data collected are then processed and interpreted using well-to-ground joint microseismic interpretation software, which enables the determination of the fracture’s azimuth, height, length, and tendency.

4. Results of Hydraulic Fracturing

4.1. Characteristics of Artificial Fracturing Fractures

Microseismic monitoring was performed on 12 fractured wells in the Baode area. As shown in Figure 2, the length of artificial fractures primarily ranges from 136 to 226 m, while their height is mainly between 8.5 and 25.3 m, accounting for 75% of the total number of fractures observed. The distribution range of fracture extension observed in microseismic monitoring is primarily concentrated between NE30° and NE64°, with a smaller distribution between NW80° and NW86° (Figure 3). The direction of fracture extension closely aligns with the principal stress direction influenced by the Himalayan structural stress field. Consequently, the dominant orientation of hydraulic fractures in the coal reservoir of the study area is toward the NE direction, indicating a strong modern geostress effect in the region.

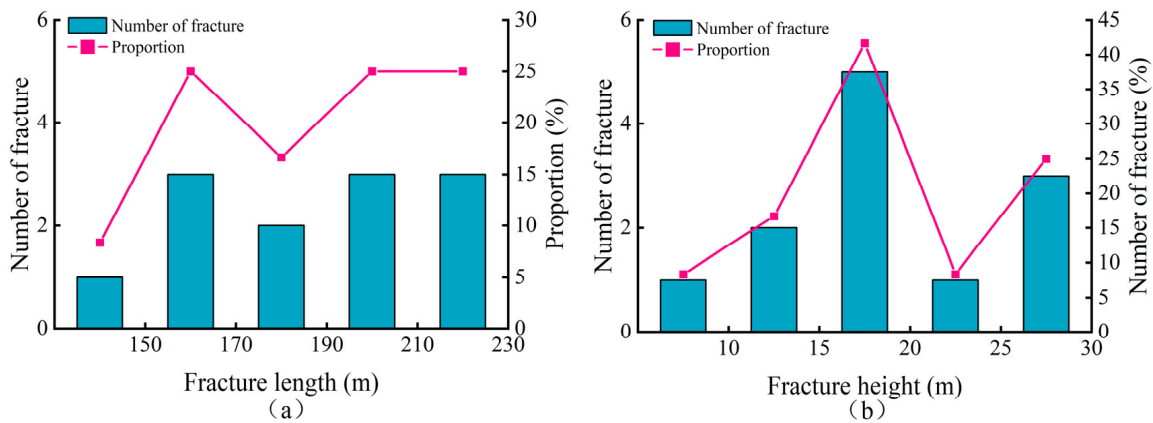


Figure 2. Microseismic monitoring of (a) fracture length distribution results and (b) fracture height distribution results.

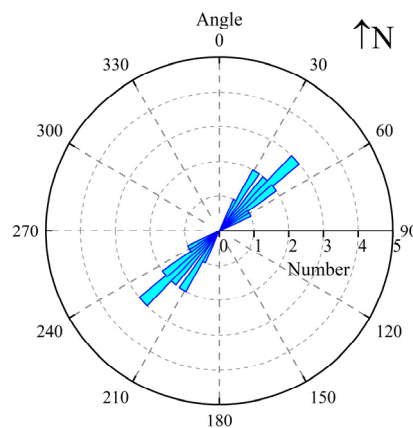


Figure 3. The orientation of hydraulic fractures according to microseismic monitoring.

4.2. Fracturing Curves

By comparing and analyzing the fracturing construction curves of over one hundred wells in the Baode Block, the construction curves for the study area were classified into four types: stable, ascending, fluctuating, and descending. This was based on the variations in the construction pressure, displacement, and sand ratio (Table 1).

The stable curve indicates that the ground construction pressure remains essentially constant over time, corresponding to steady injection displacement and consistent sand addition. This suggests that the volume of fracturing and filtration loss achieves a balance with the injection volume during the fracturing process, resulting in a generally stable pressure within the fracture. Furthermore, the fracture monitoring results demonstrate that this type of curve is associated with well-extended fractures that are long in length and conducive to effective sand addition.

Table 1. Four fracturing curves and microseismic monitoring results from Baode CBM field.

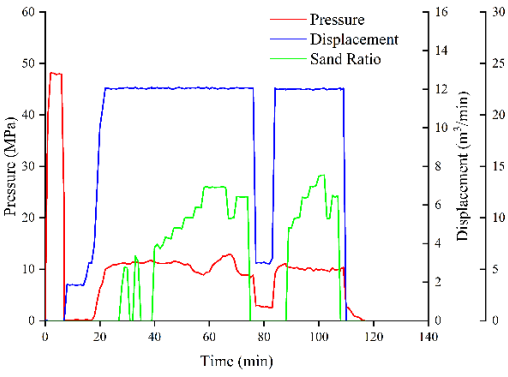
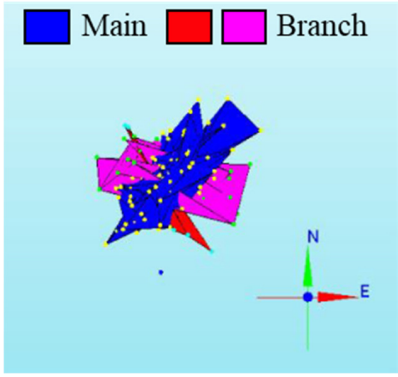
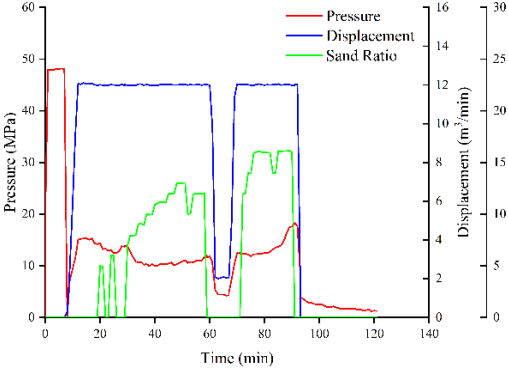
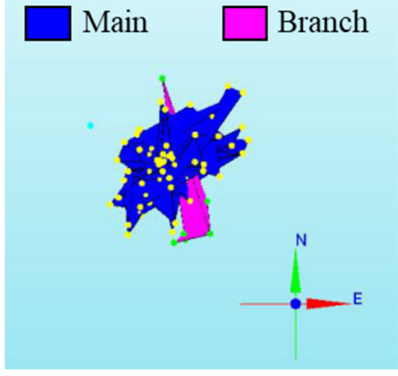
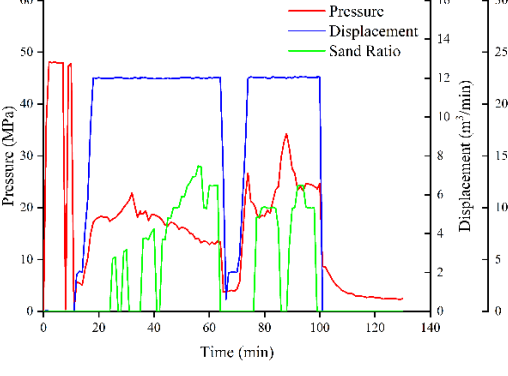
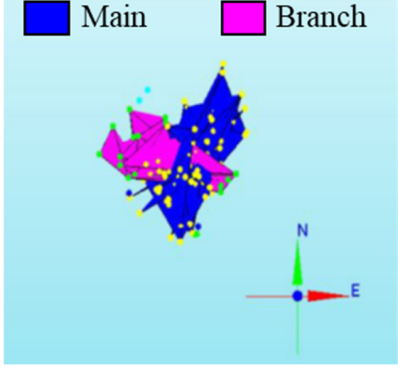
Well	Curve Type	Fracturing Curve	Fracture Monitoring	Fracture Length/m	Fracture Height/m
B1	Stable			201.25	28
B2	Ascending			136.25	24.5
B3	Fluctuating			154.25	18.5

Table 1. Cont.

Well	Curve Type	Fracturing Curve	Fracture Monitoring	Fracture Length/m	Fracture Height/m
B4	Descending			188.35	11.5

The ascending curve indicates that while the displacement stabilizes, the construction pressure continues to rise, particularly with an increased sand ratio. This suggests resistance to fracture expansion, as the rate of fracture growth and fluid loss is less than the rate of fracturing fluid injection. This resistance may arise from the complex interactions of coal structure, high reservoir pressure, and the effective sealing of the coalbed's top plate. Additionally, the fracture monitoring results reveal that the fractures associated with this curve type tend to be shorter, making sand addition during the construction process more challenging.

The fluctuating curve is characterized by constant variations in the surface pump pressure over time, despite steady discharge and sand addition. This behavior is attributed to the non-homogeneity of the permeability and stress within the coalbed, as well as the presence of natural fractures, leading to frequent changes in the filtration loss and fracture width, which in turn causes pressure fluctuations within the fractures. Consequently, this type of fracturing results in poor extension effectiveness, making it challenging to add sand during the construction process, and may even lead to sand plugging.

The declining curve exhibits stable displacement while construction pressure continuously decreases as the sand ratio increases, indicating that fracture expansion is facilitated. In this case, the rates of fracture growth and fluid loss exceed the rate of fracturing fluid injection. This phenomenon can be attributed to the better permeability of the reservoir and communication within the larger fracture or microfracture systems during the expansion process. The fracture monitoring results reveal that the extension length of the fractures associated with this curve is long, and sand addition occurs relatively easily.

5. Discussion

As shown in Figure 4, the CBM wells with longer fracture lengths and moderate fracture heights exhibit a higher gas production per meter of coal seam thickness, aligning with the findings of Yang et al. [33]. It was concluded by Yang et al. that stable fracture curves in CBM wells result in better reservoir stimulation and typically higher gas production. Therefore, when the fracturing effect and influencing factors are studied and evaluated, the length of the fracture is considered a promoting factor, while the height of the fracture is regarded as an inhibiting factor. In this way, the impact of various factors on fracture propagation and, consequently, reservoir modification is examined from both geological and engineering perspectives.

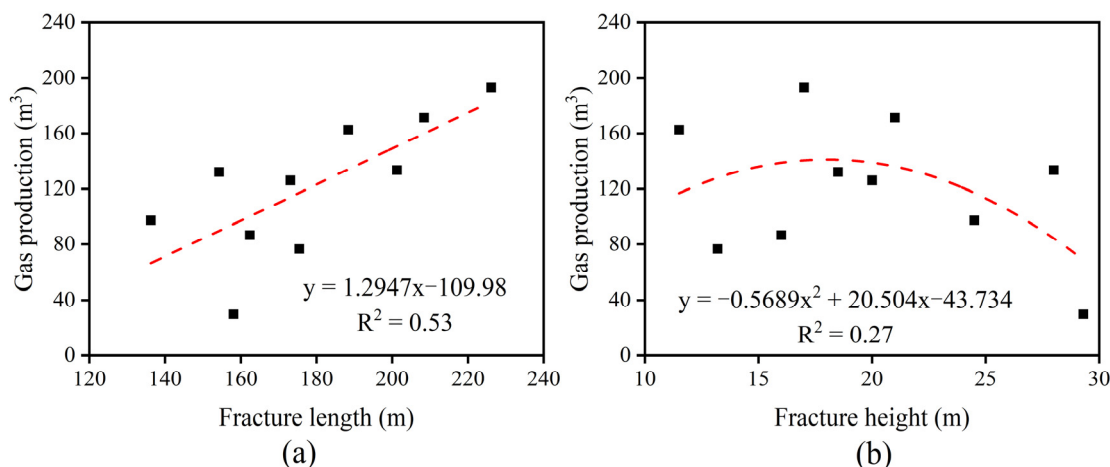


Figure 4. Relationships between gas production and (a) fracture length and (b) fracture height.

5.1. Geological Control of Hydraulic Fracture Extension

(1) Coal structure and natural fractures

Based on the damage intensity classified by the Former Soviet Union Mining Research Institute, coal structures are generally categorized into four types: undeformed coal, cataclastic coal, granulitic coal, and mylonitic coal [34]. The primary methods for identifying coal structures during CBM exploration include core observation and description, logging interpretation, and seismic inversion [35–37]. The Geological Strength Index (GSI) is a system for characterizing rock masses, introduced by Hoek et al. [38]. The determination of the GSI depends mainly on the structural integrity of the rock, the quality of fractures and joints on the structural surface of the rock structure, etc. [39]. Genzits et al. [40] and Desiman et al. [41] have used the Hoek–Brown criterion and the GSI to represent the fracturing and structure in the coal. Because logging and coring observations are the most direct and accurate means of obtaining the coal structure, the GSI is used to quantify the structural differences in the coal body in this block. The GSI value ranges from 0 to 100, which quantitatively reflects the degree of coal deformation: the larger the value of the GSI, the smaller the degree of deformation of the coal, and the closer it is to undeformed coal.

To explore the relationship between the GSI value of the coal and the fracturing effect of the coal reservoir, the coal structure was compared and analyzed alongside the microseismic monitoring results of the corresponding wells, as shown in Figure 4. The figure indicates that the fracture length during hydraulic fracturing initially increases and then decreases as the GSI increases. When the GSI value is between 60 and 65, the fracture length reaches its maximum, and the reservoir modification effect is most favorable. Based on the core drilling, logging, and GSI calculations, the coal structure in the study area is primarily composed of undeformed coal and cataclastic coal. Therefore, in this study, the coal structures are classified into four categories: undeformed coal, undeformed–cataclastic coal, cataclastic–undeformed coal, and cataclastic coal. Combined with fracture identification from electrical imaging logging, the statistical regression shows that different coal structures exhibit varying natural fracture densities (Table 2).

Table 2. Fracture density in different coal structures.

GSI	Coal Texture	Fracture Density (pcs/m)
>70	undeformed coal	1~3
60~70	undeformed–cataclastic coal	3~6
50~60	cataclastic–undeformed coal	6~9
40~50	cataclastic coal	10~15

The results indicate that natural fractures in undeformed coal ($GSI > 70$) are generally underdeveloped. While hydraulic fracturing can initiate fractures easily, these fractures tend to disperse the pumping pressure rather than concentrate it, leading to shorter fracture extension lengths (Figure 5). In the case of undeformed–cataclastic coal (GSI between 60 and 70), some natural fractures are present, and the coal structure remains relatively intact. This allows for easy rupture and the formation of stable, extended fractures during fracturing, making it the most favorable for reservoir stimulation. However, for coal structures with a higher degree of deformation ($GSI < 60$), hydraulic fracturing is highly unfavorable. The coal’s significant fragmentation, increased wetting from fracturing fluid filtration, and the mixing of coal dust with the fluid can lead to fracture blockages, severely hindering the effectiveness of the process.

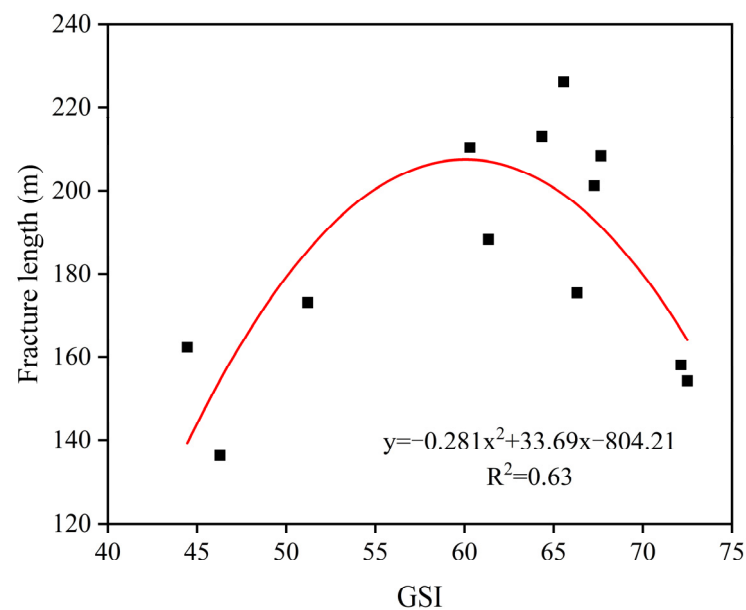


Figure 5. The relationships between GSI and fracture length.

(2) Coal macrolithotype

Based on overall relative gloss and macrocomponent content, four types of macrolithotypes can be classified: bright coal, semi-bright coal, semi-dull coal, and dull coal [42]. The primary methods for determining the macrolithotype of coal include core observation and the characterization of logging curves. However, core observation is often influenced by the varying experience levels of technicians, leading to subjective evaluation results. In contrast, there are significant differences in the logging response relationships between different macrolithotypes, making logging curves a rapid, accurate, and objective method for quantitatively characterizing coal macrolithotypes [43]. In this study, we employed a macrolithotype identification method based on logging data proposed by Cui et al. [44], which utilizes acoustic time difference, density, natural gamma, and resistivity to obtain the macrolithotype index (S_m) of coalbeds. The S_m values range from 1 to 4, with lower values indicating brighter coal in the area.

As shown in Figure 6, the study area features a rich variety of coal macrolithotypes, ranging from bright coal to dull coal. The length of the main fractures formed in the coal reservoir gradually decreases from bright coal to dull coal, while the height of the main fractures increases in the same direction. This trend can be attributed to the low mechanical strength and high brittleness of bright and semi-bright coals, which experience minimal energy loss during the fracturing process. Under appropriate hydraulic pressure, these coals tend to form main fractures that are long and narrow. In contrast, semi-dull and dull coals exhibit higher strength and greater toughness, requiring more pressure during hydraulic fracturing to promote fracture expansion. This limitation results in shorter and

taller fractures, as the hydraulic pressure is more likely to penetrate the upper and lower layers of the coal reservoir.

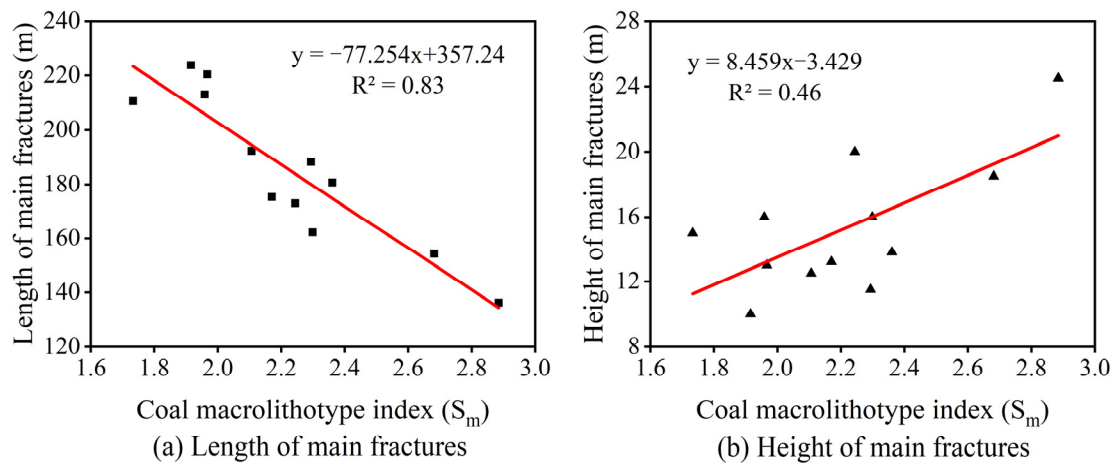


Figure 6. The relationships between coal macrolithotype index (S_m) and the length (a) and the height (b) of the main fractures.

(3) In situ stress

The in situ stress can be calculated from hydraulic fracturing data as follows [45]:

The minimum horizontal stress (σ_h) is theoretically equal to the fracture closure pressure (P_c):

$$\sigma_h = P_c \tag{1}$$

The maximum horizontal stress (σ_H) can be estimated using the following method:

$$\sigma_H = 3\sigma_h - P_f - P_o + T \tag{2}$$

where σ_H and σ_h are the maximum and minimum horizontal principal stresses, respectively; P_f is the recorded formation breakdown pressure; P_o is the pore pressure; and T is the tensile strength of rock.

The vertical stress (σ_V) can be calculated based on the integration of rock densities from the surface to the depth of coal bed:

$$\sigma_V = \int_0^Z \rho(Z)g dZ \tag{3}$$

where σ_V is the vertical stress, g is the gravitational acceleration, $\rho(Z)$ is the density as a function of depth, and Z is the depth.

As shown in Figure 7, the values of σ_H range from 8.64 to 29.59 MPa, while σ_h spans from 5.79 to 21.04 MPa, and σ_V varies between 10.83 and 38.65 MPa. Wang et al. [46] classified hydraulic fracture patterns into three categories based on the relative magnitudes of σ_H , σ_h , and σ_V : normal fault stress regime, reverse fault stress regime, and strike-slip fault stress regime (Figure 8).

In a normal fault stress regime (Figure 8a), the self-weight of the overlying rock layer exerts more influence on the coal bed than tectonic extrusion, allowing the fractures to easily expand in the vertical direction. In a reverse fault stress regime (Figure 8b), the horizontal principal stress predominates, and tectonic stress has a significant effect, leading to fracture expansion in the horizontal direction. A strike-slip fault stress regime (Figure 8c) features hydraulic fractures that are perpendicular to the direction of the maximum horizontal stress and parallel to the direction of the minimum horizontal stress, resulting in a relatively uniform extension direction characterized by predominantly vertical fractures and a narrow fracture network. Based on the relationship between the magnitudes of stress in the three

directions, the in situ stress in the study area is primarily of a normal fault stress regime, which is likely to form conjugate high-angle inclined shear fractures that align with the vertical fracture direction.

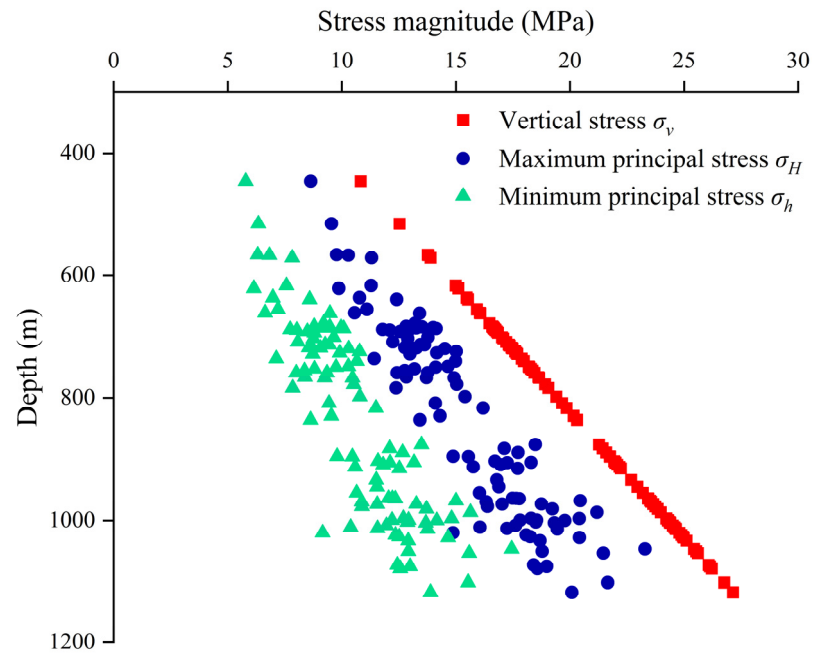


Figure 7. Relationship between in situ stress and depth.

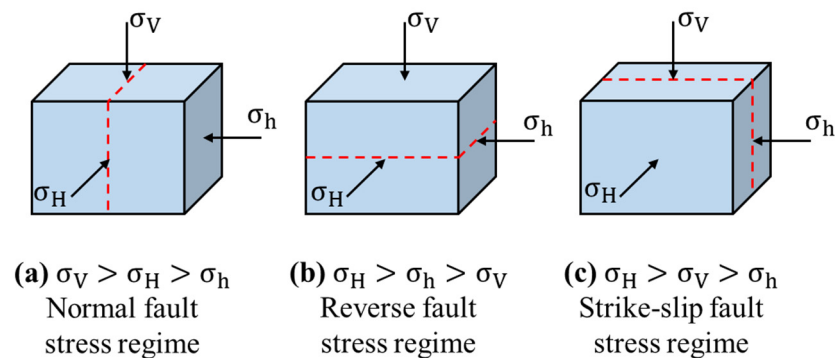


Figure 8. Relationships between hydraulic fracture and in situ stress state.

Combined with the microseismic monitoring data, the effect of differential horizontal in situ stress on fracture expansion is further analyzed. As shown in Figure 9, with an increase in the horizontal stress difference, it is observed that the length of the main hydraulic fracture gradually increases while its height decreases. Additionally, it was demonstrated by Bagheri and Settari [47] that a high level of stress difference hinders hydraulic fractures from propagating through natural fractures to form a complex fracture network. Liu et al. [48] found that when the horizontal principal stress difference is larger, hydraulic fractures are more likely to initiate and extend along orientations perpendicular to the minimum horizontal principal stress at the well wall, resulting in the formation of single fractures. The above studies indicate that when the coal bed is subjected to vertical stress, a larger difference between the two horizontal stresses facilitates the formation of long and narrow fractures, whereas a smaller difference enhances communication with natural fractures, promoting the development of a complex fracture network.

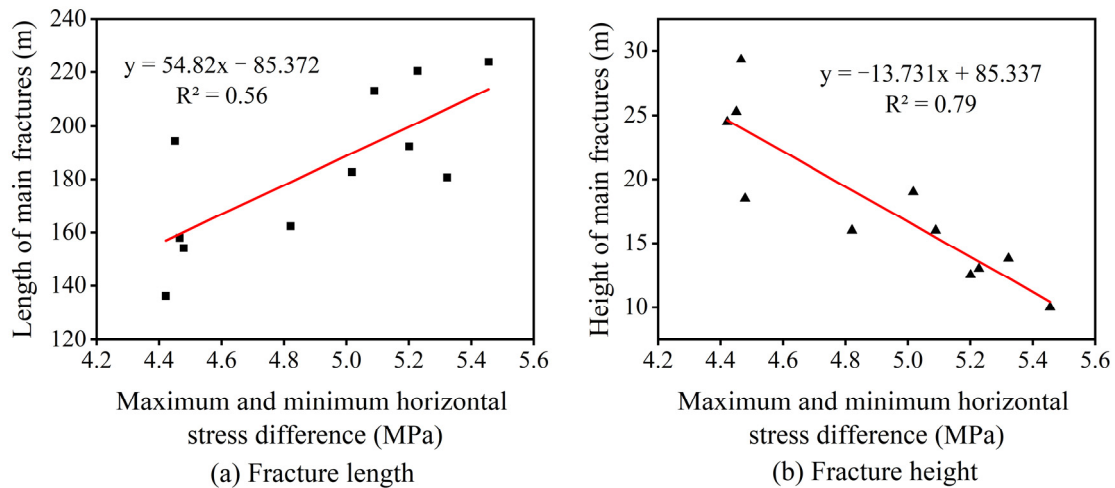


Figure 9. The relationships between $(\sigma_H - \sigma_h)$ and (a) the main fracture length and (b) height.

5.2. Engineering Control of Hydraulic Fracture Extension

The changes in the construction pressure reflect the process of fracture initiation and propagation. During hydraulic fracturing, the range of fluctuations in construction pressure varies between different CBM wells due to differences in geological conditions. As shown in Figure 10, the construction pressure ranges of the fractured wells in the study area show a statistical correlation with their fracturing characteristics. The results indicate that wells with construction pressures between 15 and 25 MPa tend to have longer average fracture lengths and lower average heights. As the construction pressure increases, the fractures progressively become wider but shorter in height.

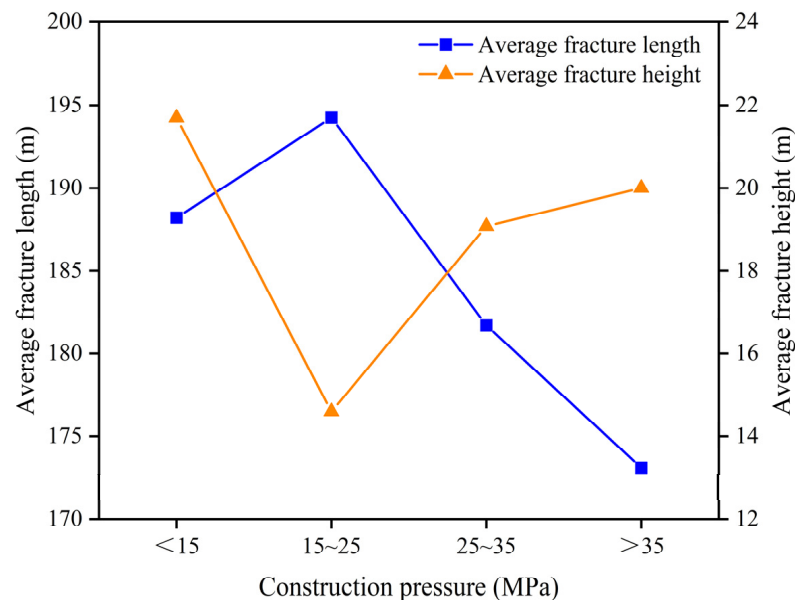


Figure 10. Relationships between construction pressure and fracture length and height.

Moreover, we analyzed the coalbed methane production under different construction pressure ranges, categorizing the stable daily gas production of the coalbed methane wells into three groups: 0–1000 m³, greater than 1000 m³, and wells with no production. The statistical results (Figure 11) indicate that the CBM wells operating at construction pressures between 15 and 25 MPa achieve the highest gas yields, with the lowest proportion of non-producing wells. In contrast, when the construction pressure exceeds 35 MPa, the daily gas production drops significantly. These findings suggest that CBM wells subjected to construction pressures in the 15–25 MPa range generate longer fractures with reduced

heights, leading to improved gas production. However, during the hydraulic fracturing process, construction pressure can be actively controlled through human intervention.

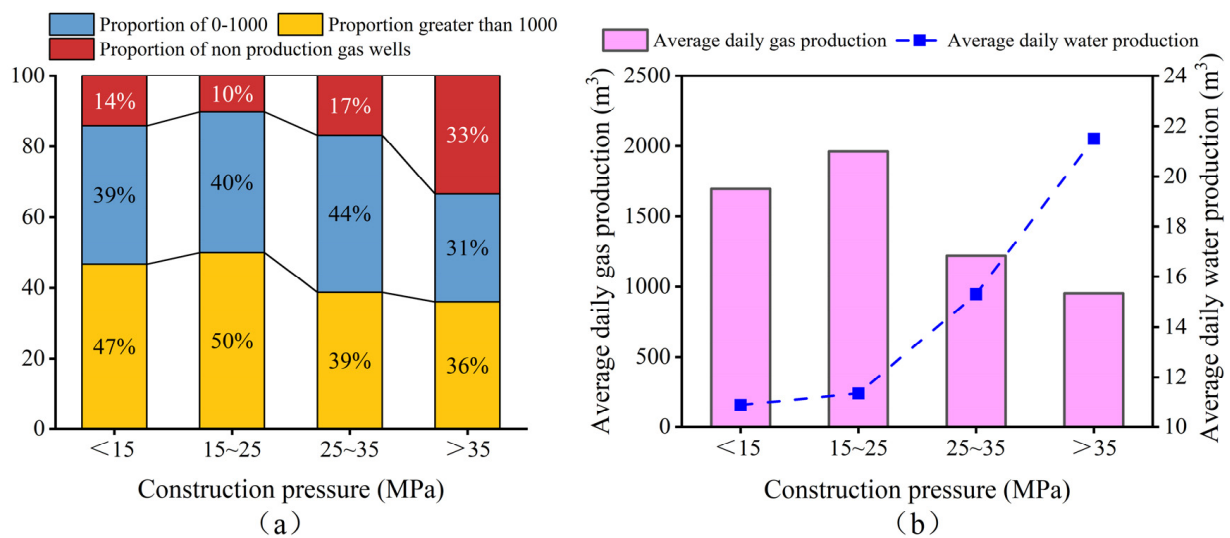


Figure 11. (a) The gas production of wells at different construction pressures; (b) average daily gas production of wells with different construction pressures.

The sand-carrying capacity of the fracturing fluid and the ability of the fracturing fluid to suspend the quartz sand will result in different concentrations of sand ratios in the wellbore and fractures, and the resulting hydrostatic pressures will be different, which will lead to fluctuations in the pressure curve. Similarly, the selection of different concentrations of proppant will also cause pressure fluctuations. During the fracturing process, a rapid increase in the sand ratio concentration, a localized high sand ratio concentration due to equipment and instrument failure, or the weakening of the sand carrying capacity of the fracturing fluid to improve the performance of the fracturing fluid when increasing the sand ratio concentration will easily lead to an increase in the construction pressure, or even the occurrence of sand plugging. In addition, the preflush ratio plays a crucial role in initiating coal seam fracturing, influencing the initial morphology of hydraulic fractures and causing fluctuations in the construction pressure. Consequently, it is possible to maintain a stable construction pressure by designing appropriate construction parameters, such as the preflush ratio, and by promptly adjusting parameters like displacements and the sand ratio in response to changes in the construction pressure during the process.

As shown in Figure 12, the length of the monitored fractures shows a parabolic correlation with the average sand ratio and preflush ratio. This suggests that fractures effectively extend when reasonable sand ratios and preflush intervals are maintained. Based on the actual research results from the study area, it is recommended to use simulated formation water as the fracturing fluid, control the preflush to be between 20% and 30% of the total fluid volume, and maintain an average sand ratio of 13% to 15%. Therefore, when the pressure curve shows a slow rise, remedial measures should be taken immediately to prevent serious issues such as sand plugging and to ensure that the fracturing process is carried out safely and smoothly.

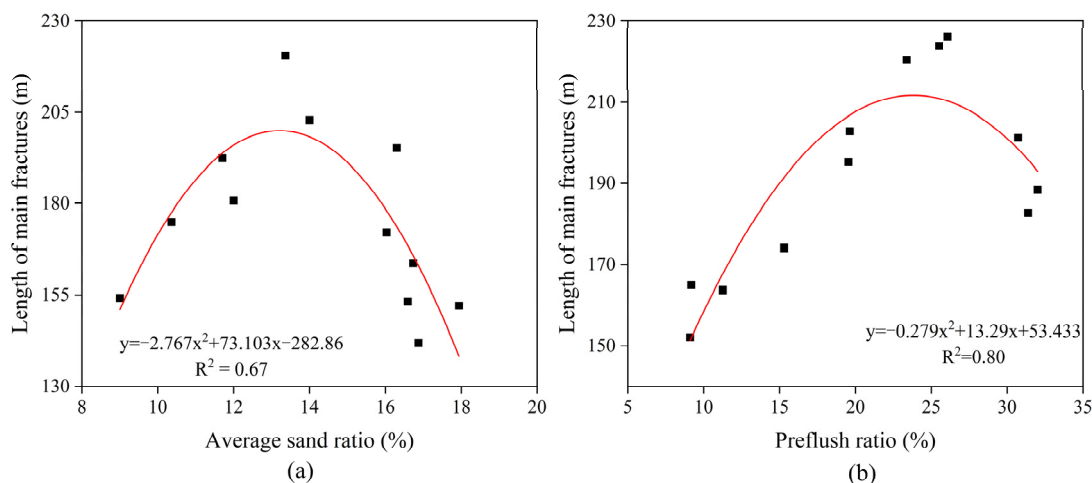


Figure 12. Relationships between fracture length and (a) average sand ratio; (b) preflush ratio.

6. Conclusions

- (1) The fracturing curves in the Baode Block are categorized into four types. Among them, the stable fracturing curve corresponds to the longest fracture length and the most effective reservoir modification, followed by the descending type. In contrast, the ascending and fluctuating types correspond to shorter, higher hydraulic fractures, yielding the poorest reservoir modification outcomes.
- (2) The natural fracture densities in undeformed–cataclastic coals typically range from 3 to 6, indicating that long hydraulic fractures are more easily formed. Bright coal and semi-bright coal, characterized by low mechanical strength and high brittleness, are more susceptible to fracturing under external forces. These properties result in longer fracture propagation distances and improved hydraulic fracturing results. Moreover, significant differences between the maximum and minimum horizontal principal stresses promote the development of long fractures.
- (3) Hydraulic fracturing operations with a preflush ratio of 20–30%, an average sand ratio of 13–15%, and a construction pressure between 15 MPa and 25 MPa are more favorable for achieving high and stable coalbed methane production.

Author Contributions: Conceptualization Y.Y. and Y.L.; methodology, Q.Z., S.W. and Z.L.; investigation, Q.Z., F.D., Z.W., Z.T. and W.Z.; writing—original draft preparation, Q.Z. and S.W.; writing—review and editing, Y.Y. and Q.Z. All authors have read and agreed to the published version of the manuscript.

Funding: This work was supported by the National Natural Science Foundation of China [42125205; 42202195] and the Fundamental Research Funds for the Central Universities [2652023001; 2652023066; 2652023204].

Data Availability Statement: The data are contained within the article.

Conflicts of Interest: Qingfeng Zhang, Yongchen Li, Ziling Li, Zebin Wang, Zhihao Tang and Wen Zhang were employed by the PetroChina Coalbed Methane Company Limited. All authors declare that the research was conducted in the absence of any commercial or financial relationships that could be construed as a potential conflict of interest.

References

1. Tao, S.; Chen, S.; Pan, Z. Current Status, Challenges, and Policy Suggestions for Coalbed Methane Industry Development in China: A Review. *Energy Sci. Eng.* **2019**, *7*, 1059–1074. [[CrossRef](#)]
2. Li, H.; Lau, H.C.; Huang, S. China’s Coalbed Methane Development: A Review of the Challenges and Opportunities in Subsurface and Surface Engineering. *J. Pet. Sci. Eng.* **2018**, *166*, 621–635. [[CrossRef](#)]
3. Li, Z.; Peng, J.; Li, L.; Qi, L.; Li, W. Novel Dynamic Multiscale Model of Apparent Diffusion Permeability of Methane through Low-Permeability Coal Seams. *Energy Fuels* **2021**, *35*, 7844–7857. [[CrossRef](#)]

4. Wanniarachchi, W.A.M.; Ranjith, P.G.; Perera, M.S.A.; Rathnaweera, T.D.; Zhang, D.C.; Zhang, C. Investigation of Effects of Fracturing Fluid on Hydraulic Fracturing and Fracture Permeability of Reservoir Rocks: An Experimental Study Using Water and Foam Fracturing. *Eng. Fract. Mech.* **2018**, *194*, 117–135. [[CrossRef](#)]
5. Sun, X.; Yao, Y.; Liu, D.; Ma, R.; Qiu, Y. Effects of Fracturing Fluids Imbibition on CBM Recovery: In Terms of Methane Desorption and Diffusion. *SPE J.* **2024**, *29*, 505–517. [[CrossRef](#)]
6. Detournay, E. Mechanics of Hydraulic Fractures. *Annu. Rev. Fluid Mech.* **2016**, *48*, 311–339. [[CrossRef](#)]
7. Adachi, J.; Siebrits, E.; Peirce, A.; Desroches, J. Computer Simulation of Hydraulic Fractures. *Int. J. Rock Mech. Min. Sci.* **2007**, *44*, 739–757. [[CrossRef](#)]
8. Li, Q.; Li, Q.; Han, Y. A Numerical Investigation on Kick Control with the Displacement Kill Method during a Well Test in a Deep-Water Gas Reservoir: A Case Study. *Processes* **2024**, *12*, 2090. [[CrossRef](#)]
9. Mendelsohn, D.A. A Review of Hydraulic Fracture Modeling—Part I: General Concepts, 2D Models, Motivation for 3D Modeling. *J. Energy Resour. Technol.* **1984**, *106*, 369–376. [[CrossRef](#)]
10. Osipov, A.A. Fluid Mechanics of Hydraulic Fracturing: A Review. *J. Pet. Sci. Eng.* **2017**, *156*, 513–535. [[CrossRef](#)]
11. Bunger, A.P.; Petroleum, C.; Detournay, E. Numerical Simulation of Hydraulic Fracturing in the Viscosity-Dominated Regime. In *SPE Hydraulic Fracturing Technology Conference and Exhibition*; SPE: Kuala Lumpur, Malaysia, 2007.
12. Chen, L.; Wang, S.; Zhang, D.; Li, R.; Lu, S. Impact of cement slurry invasion on the propagation of hydraulic fractures in coal reservoirs. *Nat. Gas Ind.* **2019**, *39*, 74–81.
13. Li, Q.; Li, Q.; Wang, F.; Wu, J.; Wang, Y. The Carrying Behavior of Water-Based Fracturing Fluid in Shale Reservoir Fractures and Molecular Dynamics of Sand-Carrying Mechanism. *Processes* **2024**, *12*, 2051. [[CrossRef](#)]
14. Li, Q.; Li, T.; Cai, Y.; Liu, D.; Li, L.; Ru, Z.; Yin, T. Research progress on hydraulic fracture characteristics and controlling factors of coalbed methane reservoirs. *J. China Coal Soc.* **2023**, *48*, 4443–4460.
15. Li, R.; Wang, S.; Li, G.; Wang, J. Influences of Coal Seam Heterogeneity on Hydraulic Fracture Geometry: An In Situ Observation Perspective. *Rock Mech. Rock Eng.* **2022**, *55*, 4517–4527. [[CrossRef](#)]
16. Liu, Y.; Tang, D.; Xu, H.; Zhao, T.; Hou, W. Effect of Interlayer Mechanical Properties on Initiation and Propagation of Hydraulic Fracturing in Laminated Coal Reservoirs. *J. Pet. Sci. Eng.* **2022**, *208*, 109381. [[CrossRef](#)]
17. Zhong, J.; Ge, Z.; Lu, Y.; Zhou, Z.; Zheng, J. New Mechanical Model of Slotting–Directional Hydraulic Fracturing and Experimental Study for Coalbed Methane Development. *Nat. Resour. Res.* **2021**, *30*, 639–656. [[CrossRef](#)]
18. Olson, J.E.; Bahorich, B.; Holder, J. Examining Hydraulic Fracture—Natural Fracture Interaction in Hydrostone Block Experiments. In *All Days*; SPE: The Woodlands, TX, USA, 2012; p. SPE-152618-MS.
19. Han, W.; Wang, Y.; Li, Y.; Ni, X.; Wu, X.; Wu, P.; Zhao, S. Recognizing Fracture Distribution within the Coalbed Methane Reservoir and Its Implication for Hydraulic Fracturing: A Method Combining Field Observation, Well Logging, and Micro-Seismic Detection. *J. Nat. Gas Sci. Eng.* **2021**, *92*, 103986. [[CrossRef](#)]
20. Zhao, H.; Wang, X.; Liu, Z. Experimental Investigation of Hydraulic Sand Fracturing on Fracture Propagation under the Influence of Coal Macrolithotypes in Hancheng Block, China. *J. Pet. Sci. Eng.* **2019**, *175*, 60–71. [[CrossRef](#)]
21. Yushi, Z.; Xinfang, M.; Shicheng, Z.; Tong, Z.; Han, L. Numerical Investigation into the Influence of Bedding Plane on Hydraulic Fracture Network Propagation in Shale Formations. *Rock Mech. Rock Eng.* **2016**, *49*, 3597–3614. [[CrossRef](#)]
22. Wanniarachchi, W.A.M.; Ranjith, P.G.; Li, J.C.; Perera, M.S.A. Numerical Simulation of Foam-Based Hydraulic Fracturing to Optimise Perforation Spacing and to Investigate Effect of Dip Angle on Hydraulic Fracturing. *J. Pet. Sci. Eng.* **2019**, *172*, 83–96. [[CrossRef](#)]
23. Ranjith, P.G.; Wanniarachchi, W.A.M.; Perera, M.S.A.; Rathnaweera, T.D. Investigation of the Effect of Foam Flow Rate on Foam-Based Hydraulic Fracturing of Shale Reservoir Rocks with Natural Fractures: An Experimental Study. *J. Pet. Sci. Eng.* **2018**, *169*, 518–531. [[CrossRef](#)]
24. Liang, Y.; Wang, M.; Luo, Y.; Rui, T.; Wang, X.; Meng, Y. Research on the Factors Influencing the Width of Hydraulic Fractures through Layers. *J. Pet. Explor. Prod. Technol.* **2024**, *14*, 2113–2127. [[CrossRef](#)]
25. Yang, D.; Ning, Z.; Li, Y.; Lv, Z.; Qiao, Y. In Situ Stress Measurement and Analysis of the Stress Accumulation Levels in Coal Mines in the Northern Ordos Basin, China. *Int. J. Coal Sci. Technol.* **2021**, *8*, 1316–1335. [[CrossRef](#)]
26. Liu, D.; Li, J.; Liu, J.; Zhang, L. Modeling Hydrocarbon Accumulation Based on Gas Origin and Source Rock Distribution in Paleozoic Strata of the Ordos Basin, China. *Int. J. Coal Geol.* **2020**, *225*, 103486. [[CrossRef](#)]
27. Guo, C.; Qin, Y.; Yi, T.; Ma, D.; Wang, S.; Shi, Q.; Bao, Y.; Chen, Y.; Qiao, J.; Lu, L. Review of the progress of geological research on coalbed methane co-production. *Coal Geol. Explor.* **2022**, *50*, 42–57.
28. Xu, F.; Zhang, W.; Li, Z.; Zhang, L.; Zhang, J.; Hou, W.; Cheng, Q.; Li, Y.; Zhang, Q.; Hao, S.; et al. Coalbed Methane Reservoir Description and Enhanced Recovery Technologies in Baode Block, Ordos Basin. *Nat. Gas Ind.* **2023**, *43*, 96–112.
29. Pu, Y.; Li, S.; Tang, D. Fracturing Construction Curves and Fracture Geometries of Coals in the Southern Qinshui Basin, China: Implication for Coalbed Methane Productivity. *ACS Omega* **2024**, *9*, 30436–30451. [[CrossRef](#)]
30. Li, H.; Chang, X. A Review of the Microseismic Focal Mechanism Research. *Sci. China Earth Sci.* **2021**, *64*, 351–363. [[CrossRef](#)]
31. Chong, Z.; Yao, Q.; Li, X.; Liu, J. Investigations of Seismicity Induced by Hydraulic Fracturing in Naturally Fractured Reservoirs Based on Moment Tensors. *J. Nat. Gas Sci. Eng.* **2020**, *81*, 103448. [[CrossRef](#)]

32. Gabry, M.A.; Gharieb, A.Y.; Soliman, M.; Eltaleb, I.; Farouq-Ali, S.M.; Cipolla, C. Advanced Deep Learning for Microseismic Events Prediction for Hydraulic Fracture Treatment via Continuous Wavelet Transform. *Geoenergy Sci. Eng.* **2024**, *239*, 212983. [[CrossRef](#)]
33. Yang, G.; Hu, W.; Tang, S.; Zhou, Z.; Song, Z. Impacts of Vertical Variation of Coal Seam Structure on Hydraulic Fracturing and Resultant Gas and Water Production: A Case Study on the Shizhuangnan Block, Southern Qinshui Basin, China. *Energy Explor. Exploit.* **2024**, *42*, 52–64. [[CrossRef](#)]
34. Li, L.; Liu, D.; Cai, Y.; Wang, Y.; Jia, Q. Coal Structure and Its Implications for Coalbed Methane Exploitation: A Review. *Energy Fuels* **2021**, *35*, 86–110. [[CrossRef](#)]
35. Teng, J.; Yao, Y.; Liu, D.; Cai, Y. Evaluation of Coal Texture Distributions in the Southern Qinshui Basin, North China: Investigation by a Multiple Geophysical Logging Method. *Int. J. Coal Geol.* **2015**, *140*, 9–22. [[CrossRef](#)]
36. Wang, Y.; Liu, D.; Cai, Y.; Yao, Y.; Pan, Z. Constraining Coalbed Methane Reservoir Petrophysical and Mechanical Properties through a New Coal Structure Index in the Southern Qinshui Basin, Northern China: Implications for Hydraulic Fracturing. *AAPG Bull.* **2020**, *104*, 1817–1842. [[CrossRef](#)]
37. Cao, L.; Yao, Y.; Liu, D.; Yang, Y.; Wang, Y.; Cai, Y. Application of Seismic Curvature Attributes in the Delineation of Coal Texture and Deformation in Zhengzhuang Field, Southern Qinshui Basin. *AAPG Bull.* **2020**, *104*, 1143–1166. [[CrossRef](#)]
38. Hoek, E.; Kaiser, P.K.; Bawden, W.F. *Support of Underground Excavations in Hard Rock*; CRC Press: Boca Raton, FL, USA, 2000.
39. Hoek, E.; Marinos, P. Predicting Tunnel Squeezing Problems in Weak Heterogeneous Rock Masses. *Tunn. Tunn. Int.* **2000**, *32*, 45–51.
40. Gentzis, T.; Deisman, N.; Chalaturnyk, R.J. Geomechanical Properties and Permeability of Coals from the Foothills and Mountain Regions of Western Canada. *Int. J. Coal Geol.* **2007**, *69*, 153–164. [[CrossRef](#)]
41. Deisman, N.; Gentzis, T.; Chalaturnyk, R.J. Unconventional Geomechanical Testing on Coal for Coalbed Reservoir Well Design: The Alberta Foothills and Plains. *Int. J. Coal Geol.* **2008**, *75*, 15–26. [[CrossRef](#)]
42. O’Keefe, J.M.K.; Bechtel, A.; Christanis, K.; Dai, S.; DiMichele, W.A.; Eble, C.F.; Esterle, J.S.; Mastalerz, M.; Raymond, A.L.; Valentim, B.V.; et al. On the Fundamental Difference between Coal Rank and Coal Type. *Int. J. Coal Geol.* **2013**, *118*, 58–87. [[CrossRef](#)]
43. Tao, S.; Pan, Z.; Chen, S.; Tang, S. Coal Seam Porosity and Fracture Heterogeneity of Marcolithotypes in the Fanzhuang Block, Southern Qinshui Basin, China. *J. Nat. Gas Sci. Eng.* **2019**, *66*, 148–158. [[CrossRef](#)]
44. Cui, C.; Chang, S.; Yao, Y.; Cao, L. Quantify Coal Macrolithotypes of a Whole Coal Seam: A Method Combing Multiple Geophysical Logging and Principal Component Analysis. *Energies* **2021**, *14*, 213. [[CrossRef](#)]
45. Ju, W.; Shen, J.; Qin, Y.; Meng, S.; Wu, C.; Shen, Y.; Yang, Z.; Li, G.; Li, C. In-Situ Stress State in the Linxing Region, Eastern Ordos Basin, China: Implications for Unconventional Gas Exploration and Production. *Mar. Pet. Geol.* **2017**, *86*, 66–78. [[CrossRef](#)]
46. Wang, R.; Pan, J.; Wang, Z.; Li, G.; Ge, T.; Zheng, H.; Wang, X. Influence of In Situ Stress on Well Test Permeability and Hydraulic Fracturing of the Fanzhuang Block, Qinshui Basin. *Energy Fuels* **2021**, *35*, 2121–2133. [[CrossRef](#)]
47. Bagheri, M.; Settari, A. Modeling of Geomechanics in Naturally Fractured Reservoirs. *SPE Reserv. Eval. Eng.* **2008**, *11*, 108–118. [[CrossRef](#)]
48. Liu, Z.; Chen, M.; Zhang, G. Analysis of the Influence of a Natural Fracture Network on Hydraulic Fracture Propagation in Carbonate Formations. *Rock Mech. Rock Eng.* **2014**, *47*, 575–587. [[CrossRef](#)]

Disclaimer/Publisher’s Note: The statements, opinions and data contained in all publications are solely those of the individual author(s) and contributor(s) and not of MDPI and/or the editor(s). MDPI and/or the editor(s) disclaim responsibility for any injury to people or property resulting from any ideas, methods, instructions or products referred to in the content.